

# Charge Transfer Characteristics of n-type $\text{In}_{0.1}\text{Ga}_{0.9}\text{N}$ Photoanode across Semiconductor–Liquid Interface

Lorenzo Caccamo,<sup>†</sup> Cristian Fabrega,<sup>‡</sup> Marcel Marschewski,<sup>§</sup> Sönke Fündling,<sup>†</sup> Alaaeldin Gad,<sup>†,⊥</sup> Olga Casals,<sup>‡</sup> Gerhard Lilienkamp,<sup>§</sup> Oliver Hoff,<sup>§,||</sup> Joan Daniel Prades,<sup>‡</sup> Winfried Daum,<sup>§</sup> and Andreas Waag<sup>\*,†</sup>

<sup>†</sup>Institute for Semiconductor Technology and Laboratory for Emerging Nanometrology, TU Braunschweig, Braunschweig 38092, Germany

<sup>‡</sup>MIND/IN2UB, Department d'Enginyeries: Electronica, Universitat de Barcelona, c. Martí Franquès 1, Barcelona 08028, Spain

<sup>§</sup>Institute of Energy Research and Physical Technologies, TU Clausthal, Leibnizstrasse 4, Clausthal-Zellerfeld 38678, Germany

<sup>||</sup>Institute of Electrochemistry, TU Clausthal, Arnold-Sommerfeld-Str. 6, Clausthal-Zellerfeld 38678, Germany

<sup>⊥</sup>Inorganic Chemistry Department, National Research Centre (NRC), Cairo, Egypt

\* Supporting Information

**ABSTRACT:** Understanding the mechanisms of charge transfer across the semiconductor/liquid interface is crucial to realize efficient photoelectrochemical devices. Here, the interfacial charge transfer characteristics of n-type  $\text{In}_{0.1}\text{Ga}_{0.9}\text{N}$  photoanodes are investigated and correlated to their photo-activity properties measured in phosphate buffered saline solution (pH 7) under illumination conditions. Cyclic voltammetry measurements show evident photoactivity changes as the number of cycles increases. In particular, the photocurrent density reaches its maximum value after 49 voltammetric cycles; meanwhile, the photocurrent onset potential shifts toward more negative cathodic potentials.

Electrochemical impedance measurements reveal that, first, the hole transfer process occurs mainly via localized states at the surface and the photocurrent onset potential is dependent on the energetic position of those states. Therefore, the observed initial photocurrent increase and cathodic shift of the photocurrent onset potential can be attributed to a decrease of the transfer resistance and partial passivation of the states at the surface. On the other hand, a gradual oxidation and corrosion of the InGaN surface arises, causing a consequential decrease of the photocurrent. At this point, the charge transfer process occurs predominantly from the valence band. This work provides a basic understanding of the charge transfer mechanisms across the InGaN/liquid interface which can be used to improve the overall photoanode efficiency.

## INTRODUCTION

In photoelectrochemical cells, the compositional and electronic properties of the semiconductor surface are closely related and influence the performance of the whole device. The role of the surface states on the charge transfer across the semiconductor–liquid interface (SLI) is of great importance, especially on how they can severely limit the photocarrier extraction, leading to an undesired overpotential.<sup>1</sup> Therefore, understanding the mechanisms of charge transfer enables one to elaborate strategies to improve the overall device efficiency.<sup>2</sup>

$\text{In}_x\text{Ga}_{1-x}\text{N}$  is a semiconductor of interest for different applications including light-emitting diodes<sup>3,4</sup> and biosensors.<sup>5</sup> In particular, InGaN has attracted a lot of attention as material<sup>6,7</sup> for photoelectrodes because of its large carrier mobility, high light absorption coefficient, and the ability to tune its band gap by tailoring the indium concentration.<sup>8,9</sup> However, the relative high overpotential of InGaN could hinder its application as photoelectrode.<sup>10</sup> One reason for that can be

found in the position of the conduction band (CB) of InGaN with respect to the hydrogen redox potential.<sup>11,12</sup> Being strongly dependent on the indium content, the CB edge lies below the hydrogen potential for relatively high indium concentrations ( $x > 0.15$ ), which leads to a decrease of the driving force for the photocarrier separation at the SLI. Nevertheless, this issue could be, in principle, solved using a tandem cell approach.<sup>13</sup> However, the observed overpotential cannot be solely explained by the position of the conduction band.

Chakrapani et al. reported an evidence of electrochemical Fermi level pinning at the GaN surface<sup>14</sup> caused by surface states which could affect the photovoltage. Moreover, Schafer et al. described the charge transfer mechanism across the GaN/ liquid interface as occurring via surface states.<sup>15</sup> Although many

investigations have been focused on GaN photoelectrodes in the past years, the charge transfer across the InGaN/liquid interface has been rarely addressed.<sup>16</sup>

In this work, we report a fundamental study to elucidate further the charge transfer mechanisms across the n-type  $\text{In}_{0.1}\text{Ga}_{0.9}\text{N}$  photoanode/liquid interface under monochromatic light conditions. The photoelectrochemical behavior of the photoanode in pH  $\sim$  7.0 phosphate buffered saline (PBS) solution was investigated by cyclic voltammetry (CV). Electrochemical impedance spectroscopy (EIS) was performed to gain further information about the charge transfer dynamics. Moreover, atomic force microscopy (AFM), Auger electron spectroscopy (AES), and ultraviolet photoelectron spectroscopy (UPS) were used to study the morphology of the InGaN surface and its chemical composition.

## EXPERIMENTAL SECTION

The n-type InGaN photoelectrodes were grown on 2 in. GaN/sapphire (0001) wafers by metal-organic vapor phase epitaxy (MOVPE) in an Aixtron 2600G3 HT reactor system. The InGaN layers were unintentionally doped. Further details of the sample growth can be found elsewhere.<sup>17</sup> The thickness of the  $\text{In}_x\text{Ga}_{(1-x)}\text{N}$  layers ( $31 \pm 0.4$  nm) and the indium content ( $x = 0.102 \pm 0.003$ ) were measured by the XRD technique with a PANalytical X'Pert system. The indium content was further confirmed by photoluminescence (PL) measurements.

The photoelectrochemical (PEC) tests were carried out in a phosphate buffered saline solution which was prepared by mixing 5.44 g of  $\text{KH}_2\text{PO}_4$  salt into 200 mL of deionized water. KOH was added to reach pH  $7.0 \pm 0.2$ . Both pH and temperature of the solution ( $21^\circ\text{C}$ ) were controlled before and after the photoelectrochemical tests. WTW pH 197 m was employed as pH meter. The solution was bubbled with nitrogen prior and during the tests to ensure low levels of dissolved oxygen in water. The samples were cut in pieces of  $\sim 1.2 \times 0.7$  cm<sup>2</sup>, and the exposed areas ( $\sim 0.5$  cm<sup>2</sup>) were delimited using an epoxy resin. The Ohmic contacts were made depositing metallic indium on the top part of the samples.

Cyclic voltammetry (CV) measurements were performed under dark and light conditions by using a three-electrode configuration; namely, a 3 M KCl Ag/AgCl electrode and a platinum wire were used as a reference electrode and counter electrode, respectively. All cyclic voltammograms (80 cycles in light condition) were recorded with a scan rate of 50 mV/s. Three light-emitting diodes (LED) with an emission wavelength of 395 nm (fwhm  $\sim$  10 nm) were employed as illumination source (low intensity), and their light was focused on the InGaN surface.

Electrochemical impedance spectra (IS) were collected applying a sinusoidal signal with an amplitude of 35 mV and a frequency range from 1 MHz to 0.5 Hz superimposed to the bias voltage. In order to investigate the charge transfer across the InGaN/liquid interface, the impedance spectra were taken over a relatively large bias potential range with an interval of 70 mV. The IS were fitted using ZView software. Furthermore, the spectra were acquired after the 1st, the 50th, and 75th CV scans and named S1, S50, and S75, respectively. Both cyclic voltammetric scans and impedance plots were recorded using an SP-150 BioLogic potentiostat.

The surface morphology of the samples was investigated using a Veeco Dimension 3100 atomic force microscope. All the surface scans were performed on an area of  $3 \times 3$   $\mu\text{m}^2$  in tapping mode employing a silicon cantilever.

AES spectra were recorded before and after the CV test using an Omicron NanoSAM setup fitted with a modified Zeiss Supra field-emission scanning electron microscope and a hemispherical electron energy analyzer. The measurements were carried out in constant retard ratio (CRR) scan mode (CRR = 4) using an electron beam with a primary energy of 5 keV as an excitation source (normal angle of incidence). The spectra were shifted using the carbon Auger peak (275.0 eV) that originated from the surface contamination to correct the energy shift caused by the sample charging. A five-point Savatzki-Golay function (SG5) was applied to all spectra.

UPS measurements were carried out in an ultra-high-vacuum (UHV) chamber with a base pressure below  $5 \times 10^{-10}$  mbar. The chamber is equipped with a combined MIES/UPS source, a commercial non-monochromatic RS40B1 Prevac X-ray source, and a hemispherical analyzer. A home-built cold-cathode He I discharge source is used to produce a radiation with characteristic energy of 21.2 eV ( $45^\circ$  angle of incidence).

The sample surfaces were placed perpendicularly to the entrance slit of the hemispherical analyzer. UPS spectra (resolution of 250 meV) are displayed as a function of the electron binding energy with respect to the Fermi level, which is determined by the high energy cutoff obtained on a Au(111) single crystal in UPS. Further details can be found elsewhere.<sup>18</sup> All samples were measured untreated and after being heated up to  $200^\circ\text{C}$  to remove most of the environmental contaminations. The native oxide on the "as-grown" sample was not removed in order to prevent damages which might have affected the measurements.

## RESULTS AND DISCUSSION

Cyclic voltammetric measurements were performed to study the electrical behavior of the n-type InGaN anode under illumination as a function of voltammetric cycles (Figure 1a).

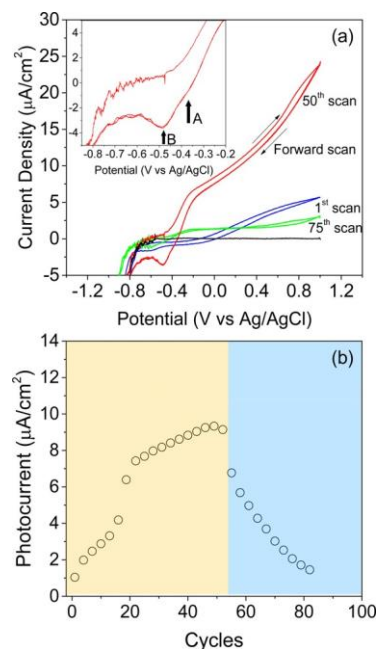


Figure 1. (a) Selected cyclic voltammograms performed under illumination (wavelength 395 nm) in PBS solution having pH 7. The CV in dark condition is also shown (black line). The inset shows the characteristic reductive peaks of CV50. (b) The photocurrent at 187 mV<sub>Ag/AgCl</sub> as a function of CV cycles.

The voltammograms show evident photoactivity changes as the number of cycles increases (only few CVs were displayed for clarity); in particular, the photocurrent onset potential (or photovoltage) shifts from 17 mV (1st scan) to -417 mV at the 75th scan. Furthermore, a relatively large hysteresis between the reverse and forward scan directions is observed in the 1st (CV1) and 50th cycles (CV50), while it is drastically reduced at the 75th scan (CV75). The observed hysteresis might be attributed to a charge/discharge process and/or a chemical/ morphological modification of the InGaN surface which might have occurred during the cycles. It is likewise important to notice that, despite that InGaN showed a photocurrent in the anodic region, no peaks attributed to the reduction of oxygen were observed in the cathodic range at any scan. Usually, such a peak is observed when oxygen is produced during the anodic scans due to the reaction between the aqueous solution and the photoholes generated in the photoanode under illumination. This indicates that InGaN did not efficiently oxidize water.

A peak (B) centered at -486 mV and a shoulder (A) at -358 mV are visible in CV50 (inset, Figure 1a). The origin of the peak B is still not clear, while the shoulder A is related to the change of the electronic occupation of localized defect states at the InGaN surface (in this work named DSS), as will be discussed later.

Finally, large photocurrent density changes were observed with the increase of the scanned voltammogram cycles. Starting from  $1.04 \mu\text{A}/\text{cm}^2$  at 187 mV, it reaches its maximum value at the 49th cycle ( $9.33 \mu\text{A}/\text{cm}^2$ ) and then rapidly decreases to  $1.45 \mu\text{A}/\text{cm}^2$  at the 80th cycle (Figure 1b).

Electrochemical impedance spectroscopy was used to elucidate the charge transfer processes occurring at the InGaN/electrolyte interface under light illumination condition. Figure 2a displays representative Nyquist plots as a function of the CV cycles. A clear change of impedance can be observed

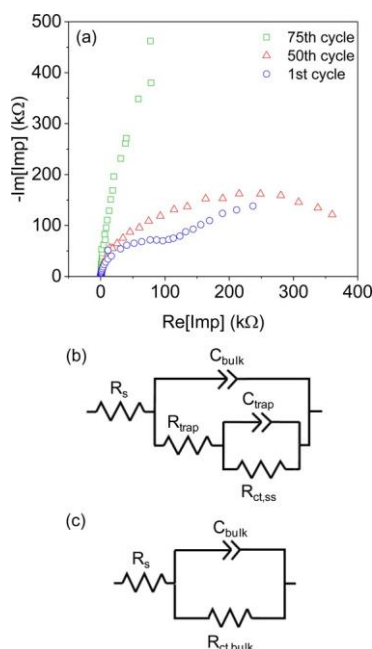


Figure 2. (a) Selected Nyquist plots recorded at 187 mV<sub>Ag/AgCl</sub> after the 1st (S1) (blue circles), 50th (S50) (red triangles), and 75th (S75) (green squares) CV cycles in light condition. (b) The equivalent circuit employed to fit the spectra S1 and S50. (c) The model used to fit the spectrum S75.

among the spectra recorded after the 1st (S1), 50th (S50), and the 75th (S75) CV scans. Two semicircles can be identified in S1 and S50, respectively, one arc at high frequency (faster process) and one arc at low frequency (slower process), while only one semicircle in S75.

Those differences of impedance are related to an alteration of the charge transfer dynamics that occurred during the CV scans. Among the models used in the literature to interpret the spectra,<sup>19,20</sup> two equivalent circuits were adopted providing consistent results. They imply two possible charge transfer processes, namely, the hole transfer into the electrolyte occurring via surface states<sup>20,21</sup> or localized defect states at the surface (indirect transfer) (Figure 2b) and hole transfer from the valence band<sup>22</sup> (direct transfer) (Figure 2c). A specific physical meaning can be assigned to each component of the proposed equivalent circuits; in particular,  $R_s$ ,  $C_{\text{bulk}}$ , and  $R_{\text{ct,bulk}}$  represent the series resistance associated with the Ohmic contacts and GaN-InGaN bulk resistances, the space-charge capacitance of the semiconductor and the Helmholtz capacitance connected in series, and the hole transfer resistance from the valence band (VB) to the electrolyte, respectively.  $R_{\text{trap}}$ ,  $R_{\text{ct,ss}}$  and  $C_{\text{trap}}$  correspond to the charge trapping resistance at the DSS, the hole transfer resistance from localized defect states at the surface, and the DSS capacitance, respectively.

Recently, Bertoluzzi et al.<sup>22</sup> have further clarified the physical

meaning of  $C_{\text{trap}}$ . When the indirect charge transfer (low bias regime) is the predominant mechanism,  $C_{\text{trap}}$  shows peaks as a function of applied bias which are related to the trapping/ detrapping of localized states at the surface, whereas, in a direct transfer (high bias regime), the capacitance is directly proportional to the hole concentration in the VB. In a real system, both transfer mechanisms might be superimposed.

Figure 3 shows the resistances and capacitances as a function of the bias potential obtained by fitting the impedance spectra S1 and S50 with the model displayed in Figure 2b, while S75 with the model in Figure 2c. The series resistance is small (in

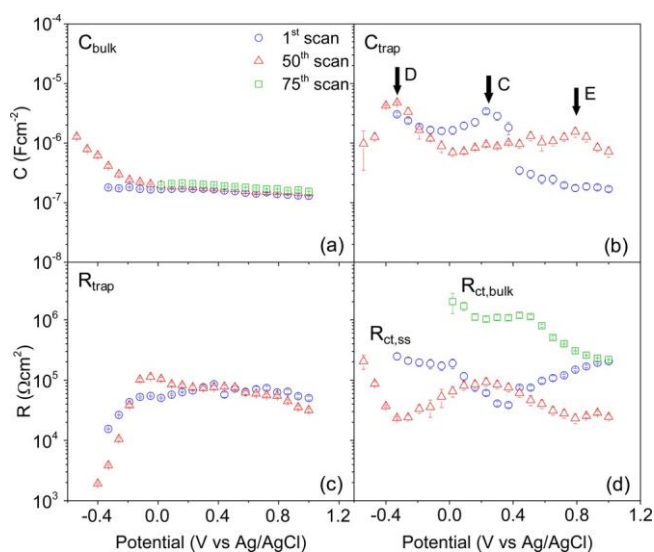


Figure 3. Calculated parameters of  $C_{\text{bulk}}$ ,  $C_{\text{trap}}$ ,  $R_{\text{trap}}$ ,  $R_{\text{ct,bulk}}$ , and  $R_{\text{ct,ss}}$  obtained by fitting the set of impedance spectra S1 (blue circles), S50 (red triangles), and S75 (green squares) with the equivalent circuits displayed in panels b and c of Figure 2. The error bars represent the uncertainties related to the fits.

the range of 25–30  $\Omega$ ) because of the conductive GaN and InGaN layers. The bulk capacitances ( $C_{\text{bulk}}$ ) decrease with the increase of the anodic bias in all three spectra (see Figure 3a). This can be explained as the result of the depletion region widening with the increase of the applied potential.

In the spectrum S1 (Figure 3b), the trap capacitance ( $C_{\text{trap}}$ ) shows one peak (C) centered at  $\sim 232$  mV and a shoulder of another expected peak in the cathodic potential range. Instead, in the spectrum S50, the peaks D and E appear at around  $-330$  and  $790$  mV, respectively, while the peak C is no longer visible.

The change of the trap capacitance after cycling reveals that the electrical properties of the InGaN were modified during the CV test. Remarkably, to each increase of  $C_{\text{trap}}$  values (Figure 3b) corresponds a decrease of the hole transfer resistance  $R_{\text{ct,ss}}$  (Figure 3d), which implies that, for the first 50 cycles, the charge transfer across the InGaN/electrolyte interface occurred predominantly via localized defect states at the surface. The higher photocurrent observed in CV50 compared to CV1 could be associated with the relative lower charge transfer resistance. The large  $R_{\text{ct,bulk}}$  compared to  $R_{\text{ct,ss}}$  confirms the low photocurrent, and hence the lower reaction rate, recorded in CV75 (see Figure 3d). In this case, the hole transfer occurred predominantly from the valence band.

$R_{\text{trap}}$  are essentially similar for S1 and S50 spectra and remain almost constant for all the anodic range (Figure 3c).

The trap capacitances ( $C_{\text{trap}}$ ) follow a Gaussian distribution.<sup>20</sup> Interestingly, the fitted peaks C ( $217 \pm 13$  mV) and D ( $-358 \pm 5$  mV) are energetically located close to their related photocurrent onset potentials (Figure 4a,b). Moreover, the

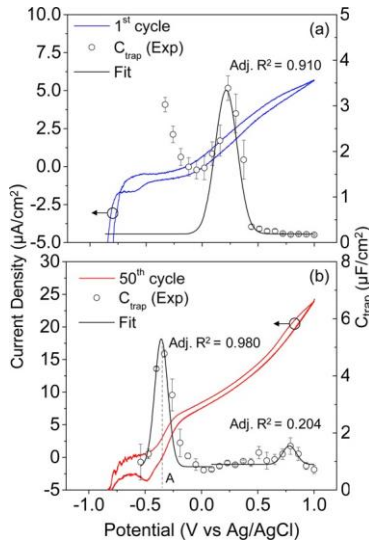


Figure 4.  $C_{\text{trap}}$  (black circles) and the Gaussian peak fit (black line) as a function of the potential after the (a) 1st (blue line) and (b) 50th (red line) CV cycles, respectively. (b) The low adjusted  $R^2$  related to the fitting of peak E could be due to the relatively scattered  $C_{\text{trap}}$  values in the region from 0.095 to 1.01  $V_{\text{Ag/AgCl}}$ .

position of the shoulder A that is visible in the 50th CV scan seems to be in correlation with the position of the capacitance peak D and could be likely related to the reduction of the DSS. The  $C_{\text{trap}}$  is associated with the density of states (DOS) through the equation shown by Monllor-Satoca et al.<sup>21</sup>

Figure 5a displays the density of DSS after the 1st and 50th scans. The peaks D and C lie within the water redox potentials and have similar DOS values, while the peak E is smaller and

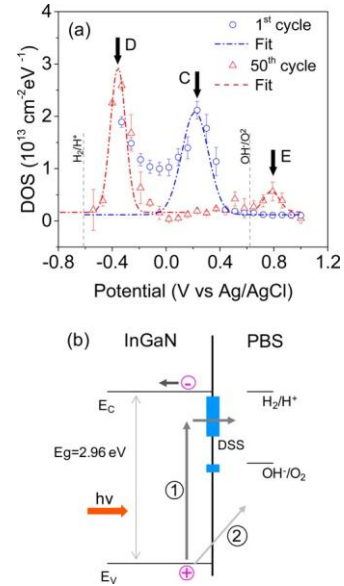


Figure 5. (a) DOS of InGaN as a function of the potential after the 1st (blue circles) and 50th CV cycles (red triangles), respectively. (b) Qualitative description of the charge transfer phenomena. Initially, the hole transfer was promoted via DSS (1), while at the end of the CV test occurred from the valence band (2).

located below the oxygen potential. As clarified by Klahr et al.,<sup>20</sup> the energetic position and the height of the DOS peaks, in our experimental conditions, are influenced by the electronic occupation of the DSS (trapping rate of electrons and holes) and correspond to the transition between the occupied and unoccupied states.<sup>22</sup>

The DOS values which have been found for the InGaN photoanode are more than 1 order of magnitude lower than the values found in similar and earlier studies performed on hematite.<sup>20,21</sup>

Figure 6a–c displays the Mott–Schottky (MS) plots extrapolated from S1, S50, and S75 spectra, respectively. The flat region observed in the MS plot (light blue-highlighted in Figure 6a) is an evidence of Fermi level pinning at the InGaN surface. This is further corroborated by the presence of the DOS in the same energetic region. The relatively high anodic photocurrent onset recorded at the first scan might find its origin in the Fermi level pinning at high anodic potentials, which reduces the ability to separate the photocarriers generated inside the semiconductor and contribute to the charge recombination.

The flatband potentials ( $E_{\text{FB}}$ ) of the InGaN photoanode after CV50 and CV75 in light condition were estimated from the linear regions of the Mott–Schottky plots. The  $E_{\text{FB}}$  shifted from  $-441 \pm 36$  mV to  $-769 \pm 50$  mV. It is interesting to notice that the InGaN photovoltage (and to some extent, also  $E_{\text{FB}}$ ) is severely limited to low cathodic potentials (or high anodic potentials for CV1) and it is intimately correlated with the energetic position of the DSS (ultimately by the Fermi level position at the surface) (Figure 4b).

The surface morphology of the InGaN photoanode before the CV test is shown in Figure 7a. Small dots can be clearly observed. After the CV test, the surface encountered a clear morphological modification as a consequence of the poor stability of the InGaN photoanodes in PBS solution at pH 7, as reported recently (Figure 7b).<sup>17</sup>

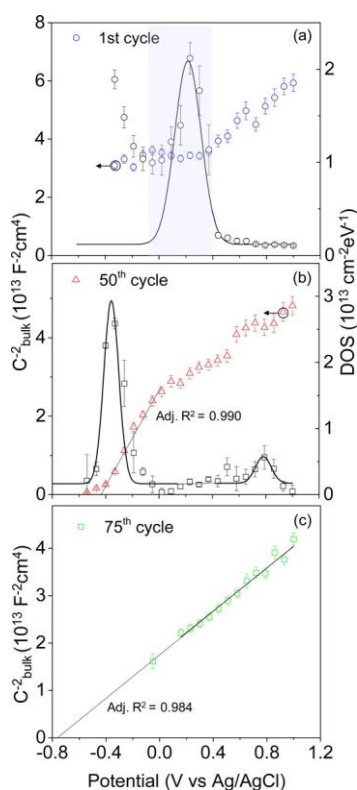


Figure 6. Mott-Schottky plots after the (a) 1st (blue circle), (b) 50th (red triangles), and (c) 75th CV cycles. The DOS (black circles) are also displayed with their relative fits (black line).

The impedance measurements allowed gaining an insight into the charge transfer mechanisms and elucidate peculiar photoelectrochemical properties of the InGaN photoanodes. During the first 50 cycles, the hole transfer across the InGaN/ PBS interface was mainly promoted through localized states at the surface (Figure 5b). The initial increase of photocurrent (yellow area, Figure 1b) and the cathodic shift of the photocurrent onset to  $-348$  mV (Figure 1a) observed during the CV test could be attributed to the progressive reduction of the transfer resistance and the states centered at 217 mV (peak C) which were acting as recombination centers and causing the Fermi level pinning at relatively high anodic potentials.

The unfavorable energetic position of the peaks C and D for the oxygen evolution reaction (Figure 5a) and the absence of the reduction peak of oxygen during the CV test suggest that the observed photocurrent was the result of the surface oxidation and corrosion. In fact, both chemical and structural properties of the InGaN surface have drastically changed during the CV test with a subsequent mixed oxide formation, as revealed by AES and UPS measurements (Supporting Information, Figures S1 and S2a,b). Furthermore, the decrease of photocurrent (blue area, Figure 1b) recorded after the 50th CV cycle might be attributed to the formation of the oxide layer at the InGaN surface. The difference of valence band offset among  $\text{In}_{0.1}\text{Ga}_{0.9}\text{N}$  and formed oxide yields to a barrier which opposes to the photohole flow from the InGaN layer to the electrolyte at low bias voltages, as also described in detail in a previous work.<sup>17</sup> Despite the photocurrent reduction, the photovoltage further shifted to  $-417$  mV at the 75th cycle. At the end of the CV test, the hole transfer occurred prevalently from the valence band (Figure 5b). This change of transfer mechanism could be attributed to the presence of a relatively

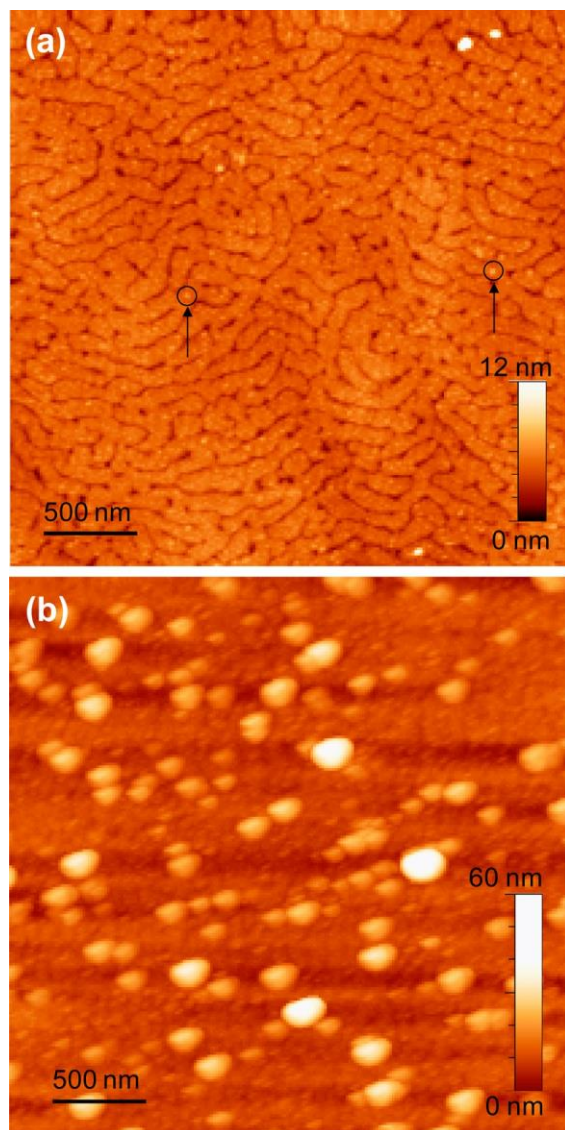


Figure 7. AFM images of the sample before (a) and after (b) the CV investigation.

thick oxide layer which probably contributed to reduce further the DSS and modified the electrical characteristics of the InGaN surface.

The origin of the observed states remains unclear, although some hypothesis can be formulated in this regard. Such states can be correlated to the structure and/or chemical composition of the InGaN surface. In his work, Van de Walle et al.<sup>23</sup> identified the origin of two groups of surface states lying within the band gap of c-polar n-GaN. The states close to the conduction band were considered unoccupied and generally associated with dangling bonds on the Ga adatoms and threefold-coordinated Ga surface atoms, while the occupied states close to the valence band were related to an electronic charge density localized among the Ga adatom and three Ga surface atoms. However, it is unlikely to observe such surface states in a complex semiconductor/liquid interface where oxidation processes and adsorbates have a great impact on the surface reconstruction, as shown by Auger spectra.

Native surface oxides are usually defective and have an important influence on the electrical properties of the interfaces. Dong et al.<sup>24</sup> observed tail states (TS) extending

from the GaN valence band in the band gap that was ascribed to the thin oxide layer formed on the GaN surface. Similarly, these tails were also noticed in the UPS spectra before and after the CV tests (Supporting Information, Figure S2a,b). However, it is difficult to correlate the defect states observed in photoelectrochemical tests (PEC) with TS because, despite the DSS suppression or passivation at the end of the PEC tests, this tail was still visible in the UPS spectrum.

The small dots on the InGaN surface observed before the CV tests (black circles, Figure 7a) might be related to the surface corrugation<sup>25</sup> or the formation of In-rich InGaN dots occurring in relatively thick layers which might introduce defect states at the surface and act as recombination centers, as also noticed by Li et al.<sup>16</sup> The possible dissolution of such defects and modification of the surface morphology could be the cause of the alteration of the hole transfer mechanisms and electric properties observed in this work.

Another possible source of localized defect states at the surface could be attributed to adsorbed species (e.g., OH groups) at the SLI which might have played a role in the chemical reactions occurring at the InGaN/liquid interface and acted as mediators for the charge transfer. It cannot be excluded that, subsequently to the morphological changes of the InGaN surface, a possible redistribution of the adsorbed species occurred, altering the charge transfer mechanisms.<sup>22</sup>

Further investigations are needed to understand the origin of these states, the correlation between the surface morphology and charge transfer, and the implications of the indium content on the transfer mechanisms.

## CONCLUSION

The charge transfer mechanisms across the n-type  $\text{In}_{0.1}\text{Ga}_{0.9}\text{N}$ /liquid interface were investigated under illumination condition employing cyclic voltammetry and electrochemical impedance spectroscopy techniques. Initially, the hole transfer process was mainly mediated by localized defect states at the surface. Those states were found to be detrimental for the InGaN photo-activity, causing a reduced photocurrent and low photovoltage. The photocurrent onset potential was found to be dependent on the energetic position of the states. The initial photocurrent increase and cathodic shift of the photocurrent onset potential with the increase of the CV cycles was attributed to the passivation (or removal) of the surface defects. On the other hand, the gradual oxidation of the InGaN surface during the photoelectrochemical process caused the decrease of the photocurrent as the number of voltammogram cycles further increased. At this point, the charge transfer process was found to occur from the valence band. A basic understanding of the charge transfer mechanisms has been provided, enabling one to elaborate in-depth strategies to improve the overall photoanode efficiency.

Corresponding Author

\*E-mail: a.waag@tu-braunschweig.de. Phone: 0049 531 3913773.

## ACKNOWLEDGMENTS

We gratefully acknowledge support by the Braunschweig International Graduate School of Metrology B-IGSM and the DFG Research Training Group GrK1952/1 "Metrology for Complex Nanosystems". The research has received funding from the European Research Council under the European Union's Seventh Framework Programme (FP/2007-2013)/ ERC Grant Agreement n. 336917. J.D.P. acknowledges support from the Serra Hunter Programme.

## REFERENCES

- (1) Bard, A. J.; Bocarsly, A. B.; Fan, F. R. F.; Walton, E. G.; Wrighton, M. S. The Concept of Fermi Level Pinning at Semiconductor/Liquid Junctions. Consequences for Energy Conversion Efficiency and Selection of Useful Solution Redox Couples in Solar Devices. *J. Am. Chem. Soc.* 1980, *102*, 3671–3677.
- (2) Le Formal, F.; Tetreault, N.; Cornuz, M.; Moehl, T.; Gratzel, M.; Sivula, K. Passivating Surface States on Water Splitting Hematite Photoanodes with Alumina Overlayers. *Chem. Sci.* 2011, *2*, 737.
- (3) Kolper, C.; Sabathil, M.; Römer, F.; Mandl, M.; Strassburg, M.; Witzigmann, B. Core-Shell InGaN Nanorod Light Emitting Diodes: Electronic and Optical Device Properties. *Phys. Status Solidi A* 2012, *209*, 2304–2312.
- (4) Ledig, J.; Wang, X.; Fündling, S.; Schuhmann, H.; Seibt, M.; Jahn, U.; Wehmann, H.-H.; Waag, A. Characterization of the Internal Properties of InGaN/GaN Core-Shell LEDs. *Phys. Status Solidi A* 2016, *213*, 11–18.
- (5) Bain, L. E.; Jewett, S. a.; Mukund, A. H.; Bedair, S. M.; Paskova, T. M.; Ivanisevic, A. Biomolecular Gradients via Semiconductor Gradients: Characterization of Amino Acid Adsorption to  $\text{InxGa1-xN}$  Surfaces. *ACS Appl. Mater. Interfaces* 2013, *5*, 7236–7243.
- (6) Caccamo, L.; Hartmann, J.; Fabrega, C.; Estrade, S.; Lilienkamp, G.; Prades, J. D.; Hoffmann, M. W. G.; Ledig, J.; Wagner, A.; Wang, X.; et al. Band Engineered Epitaxial 3D GaN-InGaN Core-Shell Rod Arrays as an Advanced Photoanode for Visible-Light-Driven Water Splitting. *ACS Appl. Mater. Interfaces* 2014, *6*, 2235–2240.
- (7) Alvi, N. u. H.; Soto Rodriguez, P. E. D.; Aseev, P.; Gomez, V. J.; Alvi, A. U. H.; Hassan, W. U.; Willander, M.; Nötzel, R. InN/InGaN Quantum Dot Photoelectrode: Efficient Hydrogen Generation by Water Splitting at Zero Voltage. *Nano Energy* 2015, *13*, 291–297.
- (8) Hahn, C.; Zhang, Z.; Fu, A.; Wu, C. H.; Hwang, Y. J.; Gargas, D. J.; Yang, P. Epitaxial Growth of InGaN Nanowire Arrays for Light Emitting Diodes. *ACS Nano* 2011, *5*, 3970–3976.
- (9) Bolton, J. R.; Strickler, S. J.; Connolly, J. S. Limiting and Realizable Efficiencies of Solar Photolysis of Water. *Nature* 1985, *316*, 495–500.
- (10) Hwang, Y. J.; Wu, C. H.; Hahn, C.; Jeong, H. E.; Yang, P. Si/InGaN Core/shell Hierarchical Nanowire Arrays and Their Photoelectrochemical Properties. *Nano Lett.* 2012, *12*, 1678–1682.
- (11) Fujii, K.; Kusakabe, K.; Ohkawa, K. Photoelectrochemical Properties of InGaN for H<sub>2</sub> Generation from Aqueous Water. *Jpn. J. Appl. Phys.* 2005, *44*, 7433–7435.
- (12) Pendyala, C.; Jasinski, J. B.; Kim, J. H.; Vendra, V. K.; Lisenkov, S.; Menon, M.; Sunkara, M. K. Nanowires as Semi-Rigid Substrates for Growth of Thick,  $\text{InxGa1-xN}$  ( $X > 0.4$ ) Epi-Layers without Phase

Segregation for Photoelectrochemical Water Splitting. *Nanoscale* 2012, 4, 6269.

(13) Fan, S.; AlOtaibi, B.; Woo, S. Y.-M.; Wang, Y.; Botton, G. A.; Mi, Z. High Efficiency Solar-to-Hydrogen Conversion on a Monolithically Integrated InGaN/GaN/Si Adaptive Tunnel Junction Photo-cathode. *Nano Lett.* 2015, 15, 2721–2726.

(14) Chakrapani, V.; Pendyala, C.; Kash, K.; Anderson, A. B.; Sunkara, M. K.; Angus, J. C. Electrochemical Pinning of the Fermi Level: Mediation of Photoluminescence from Gallium Nitride and Zinc Oxide. *J. Am. Chem. Soc.* 2008, 130, 12944–12952.

(15) Schafer, S.; Koch, A. H. R.; Cavallini, A.; Stutzmann, M.; Sharp, I. D. Charge Transfer across the N-Type GaN – Electrolyte Interface. *J. Phys. Chem. C* 2012, 116, 22281–22286.

(16) Li, M.; Luo, W.; Liu, B.; Zhao, X.; Li, Z.; Chen, D.; Yu, T.; Xie, Z.; Zhang, R.; Zou, Z. Remarkable Enhancement in Photocurrent of In<sub>0.20</sub>Ga<sub>0.80</sub>N Photoanode by Using an Electrochemical Surface Treatment. *Appl. Phys. Lett.* 2011, 99, 112108.

(17) Caccamo, L.; Cocco, G.; Martin, G.; Zhou, H.; Fundling, S.; Gad, A.; Mohajerani, M. S.; Abdelfatah, M.; Estrade, S.; Peiro, F.; et al. Insights into Interfacial Changes and Photoelectrochemical Stability of In<sub>x</sub>Ga<sub>1-x</sub>N (0001) Photoanode Surfaces in Liquid Environments. *ACS Appl. Mater. Interfaces* 2016, 8, 8232–8238.

(18) Marschewski, M.; Otto, C.; Wegewitz, L.; Höfft, O.; Schmidt, A.; Maus-Friedrichs, W. Adsorption Analysis of Thin Films of Terephthalic Acid on Au and Al Studied by MIES, UPS and XPS. *Appl. Surf. Sci.* 2015, 339, 9–14.

(19) Li, M.; Luo, W.; Liu, Q.; Zhuang, Z.; Li, Z.; Liu, B.; Chen, D.; Zhang, R.; Yu, T.; Zou, Z. An Efficient In<sub>0.30</sub>Ga<sub>0.70</sub>N Photoelectrode by Decreasing the Surface Recombination Centres in a H<sub>2</sub>SO<sub>4</sub> Aqueous Solution. *J. Phys. D: Appl. Phys.* 2013, 46, 345103.

(20) Klahr, B.; Gimenez, S.; Fabregat-Santiago, F.; Hamann, T.; Bisquert, J. Water Oxidation at Hematite Photoelectrodes: The Role of Surface States. *J. Am. Chem. Soc.* 2012, 134, 4294–4302.

(21) Monllor-Satoca, D.; Bartsch, M.; Fabrega, C.; Genc, A.; Reinhard, S.; Andreu, T.; Arbiol, J.; Niederberger, M.; Morante, J. R. What Do You Do, Titanium? Insight into the Role of Titanium Oxide as a Water Oxidation Promoter in Hematite-Based Photoanodes. *Energy Environ. Sci.* 2015, 8, 3242–3254.

(22) Bertoluzzi, L.; Lopez-Varo, P.; Jimenez Tejada, J. A.; Bisquert, J. Charge Transfer Processes at the Semiconductor/electrolyte Interface for Solar Fuel Production: Insight from Impedance Spectroscopy. *J. Mater. Chem. A* 2016, 4, 2873–2879.

(23) Van De Walle, C. G.; Segev, D. Microscopic Origins of Surface States on Nitride Surfaces. *J. Appl. Phys.* 2007, 101, 081704.

(24) Dong, Y.; Feenstra, R. M.; Northrup, J. E. Electronic States of Oxidized GaN(0001) Surfaces. *Appl. Phys. Lett.* 2006, 89, 171920.

(25) Liliental-Weber, Z.; Yu, K. M.; Bedair, S.; Zakharov, D. Planar Defects in Thin Films of InGaN. *Microsc. Microanal.* 2012, 18, 1486–1487.